



On Wake Analysis of Flow Past Rotating Downstream Cylinder using Hilbert-Huang Transformation

M. Neeraj Paul and S. Tiwari [†]

Department of Mechanical Engineering, IIT Madras, Chennai, 600036, India

[†]Corresponding Author Email: shaligt@iitm.ac.in

(Received November 20, 2017; accepted July 23, 2018)

ABSTRACT

Two-dimensional numerical simulations have been carried out on flow past two inline circular cylinders with rotating downstream cylinder. Computations are performed for fixed Reynolds number equal to 150 such that the resulting flow field remains laminar and two-dimensional. The inter-cylinder spacing has been chosen equal to $5d$ (d being diameter of cylinder) such that the wake flow is predominantly unsteady. Rotational speed of the downstream cylinder has been varied to investigate its effect on transition in characteristics of temporal wake. This has been achieved by performing Hilbert-Huang transformation (HHT) on time series signals of drag and lift coefficients for the rotating cylinder. Unsteady periodic, unsteady non-periodic and steady transitions in flow behavior have been observed with an increase of rotational speed. Results are presented in the form of vorticity contours, Hilbert spectra and marginal spectra. Degree of stationarity of the signals as measure of nonlinearity has also been quantified. Comparisons are drawn against results from Fourier analysis and it has been shown that HHT is better suited to capture inter-wave and intra-wave modulations indicating nonlinear interactions in the wake.

Keywords: Rotating downstream circular cylinder; Flow transition; spectral analysis; Hilbert-Huang transformation.

NOMENCLATURE

C_l	lift coefficient	p	static pressure
C_d	drag coefficient	p_∞	ambient pressure (exit pressure)
d	cylinder diameter	Re	Reynolds number
$DS(f)$	degree of stationarity	s	inter cylinder spacing
$EI(t)$	instantaneous energy distribution	S_C	critical drag inversion spacing
EMD	Empirical Mode Decomposition	S_r	Strouhal number
FT	Fourier Transform	t	time
f	instantaneous frequency	U_∞	free stream velocity
$H(t)$	Hilbert transform of a signal	\vec{u}	velocity vector
$H(f,t)$	hilbert spectral energy distribution		
HHT	Hilbert-Huang Transformation	α	non-dimensional rotational speed
IF	Instantaneous Frequency	ρ	density of fluid
IMF	Intrinsic Mode Function	ω	angular velocity of cylinder
$M(f)$	marginal spectral distribution	ν	kinematic viscosity
N_c	number of nodes on cylinder surface		

1. INTRODUCTION

All processes in our real world have a natural tendency to contribute towards disorder. Likewise, an apparently streamlined flow is known to transit to turbulence with an increase in driving force. Instabilities are triggered generating fluctuations

that grow and overpower its calm nature. Hence, it is essential to resolve these fluctuations in order to expose their causatives. The scales of these fluctuations provide valuable information about the underlying mechanisms. The present study attempts to interpret the transitions in flow past tandem circular cylinders with rotating downstream

cylinder using Hilbert spectral analysis. The interference between the wakes of cylinders and the effect of continuous supply of rotational energy has been observed to sustain flow transitions of both periodic and aperiodic nature.

Flow past tandem circular cylinders in the transitional regime has been subject of significant research attention during past two decades. These include studies by [Carmo and Meneghini \(2006\)](#), [Mizushima and Suehiro \(2005\)](#), [Bearman \(2011\)](#), to name a few. [Carmo and Meneghini \(2006\)](#) performed two-dimensional as well as three-dimensional computations to investigate the mechanism of wake transition in Reynolds number (Re) range of 160-320 with inter-cylinder spacing (center-to-center distance) varying from 1.5d to 8d ('d' being diameter of either cylinder). It is reported that the interference caused by proximity of the downstream cylinder curtails the development of upstream cylinder wake causing deviations in the nature of variation of force coefficients (Cd and Cl) and Strouhal number (St). They also reported that three-dimensional effects become significant only beyond Re = 190. [Mizushima and Suehirs \(2005\)](#) have numerically investigated the instabilities that appear in flow past tandem circular cylinders at Re = 100 by varying the inter-cylinder space. Bifurcation and transition diagrams have been presented by carrying out a linear stability analysis by introducing perturbations in the normal velocity component. [Bearman \(2011\)](#) has reviewed the flow characteristics and vibrations induced in flow past a pair of tandem circular cylinders. The effects due to interference between the cylinder wakes and the consequent forces developed while downstream cylinder is fixed and free to oscillate are outlined in the review.

Unlike stationary cylinders, rotational motion introduces additional complexity into the flow problem. For example, the study performed by [Mittal and Kumar \(2003\)](#) on flow past a rotating cylinder reports multiple occurrences of transitions in wake stability. Recently, [Shafi and Vengadesan \(2014\)](#) have investigated combined effects of rotational motion and interference due to the tandem arrangement. They have simulated two-dimensional flow past rotating upstream control rod by varying the inter-cylinder space, blockage ratio and rotational speed. They have referred the rotating upstream cylinder of the same size as the downstream cylinder as control rod, emphasizing on the aspects of drag reduction and vibration control. Few researchers have studied the arrangement of a rotating cylinder in the wake of an upstream cylinder ([Mittal, 2001](#); [Mittal and Raghuvanshi, 2001](#)). However, their studies have been focused on the control aspects of the wake with rotating control rods that are smaller than the primary cylinder. The interference effects between the upstream wake and the rotating downstream cylinder still remain unanswered. Moreover, at large inter-cylinder spacing (impingement range), the periodic shedding of the upstream cylinder is expected to disrupt the effects of rotation that could give rise

to transitions in periodicity.

The dynamics of vortex shedding can be analyzed by studying the time series signals of force coefficients for which conventionally Fourier spectra are employed. However, the technique falls short in accuracy when the signals are susceptible to effects of nonlinearity and high levels of modulation ([Huang et al., 1998](#)). Such effects become prominent as the flow evolves towards turbulence or due to the presence of sources that sustain mechanisms of different time scales. [Huang et al. \(1998\)](#) and [Huang et al. \(1999\)](#) proposed that the Hilbert-Huang transformation (HHT) is an effective technique to resolve complex transient signals involving multiple harmonics. This technique is reported to be free from spurious harmonics that apparently distort the results obtained from Fourier and wavelet analysis. [Sun et al. \(2006\)](#) have used HHT to eliminate background noise in order to extract the vortex shedding frequency from raw data of vortex flow meters. They concluded that HHT is better at denoising than the Fourier counterpart (FFT). Recently, it has been used by [Paul et al. \(2014\)](#) to determine the phase shift and instantaneous frequency for the case of flow past unconfined elliptic cylinders. A promising aspect of HHT is the decomposition of time series signal into a time-frequency-energy domain that discloses the instantaneous distribution of energy densities over the frequency range. The present work highlights the use of this technique for analysis of transient fluid flow problems.

Objective of the present study is to analyze the transient characteristics of unsteady wake in flow past tandem circular cylinders with rotating downstream cylinder using HHT. The rotational speed of the downstream cylinder has been varied for fixed values of inter-cylinder spacing and Re. Here the inter-cylinder spacing (s) refers to distance between centers of the cylinders and is chosen such that there is complete vortex shedding in the inter-cylinder gap in case of tandem stationary circular cylinders. Such a flow regime in which the shed vortices impinge on downstream cylinder is identified as 'impingement regime' and the critical spacing associated with such transition is called 'drag inversion spacing' (S_c) ([Igarashi, 1981](#)). The choice of Re (= 150) is based on validity of two-dimensional assumptions ([Carmo and Meneghini, 2006](#)). Such a choice ensures existence of multiple time scales, one corresponding to impingement frequency and the other to the frequency of rotation. The interaction between these frequencies is bound to create transients of complex nature. Hence, HHT is employed to interpret these signals by transforming these to frequency-energy-time domain. Empirical Mode Decomposition (EMD) has been used to identify the component signals while their Hilbert transform brings out associated energy signature. This allows extraction of dominant component signals that are associated with strong disturbances while neglecting low energy high-frequency fluctuations.

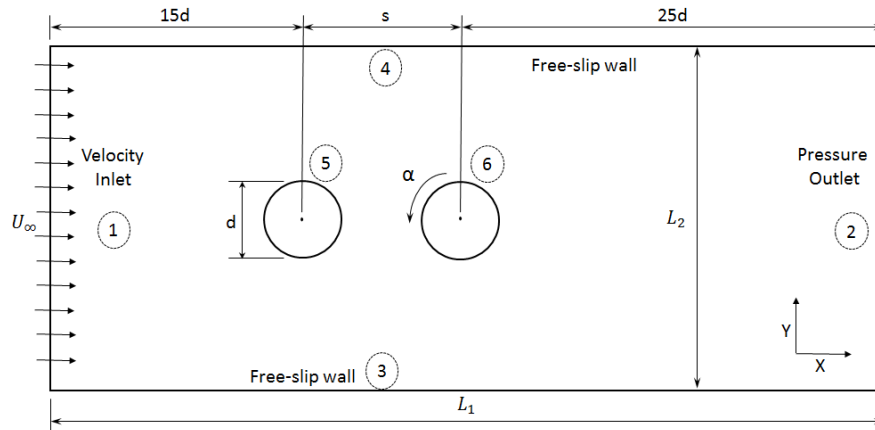


Fig. 1. Computational domain.

2. PROBLEM DEFINITION

Schematic diagram of the computational domain is presented in Fig. 1. The stationary upstream cylinder is located $15d$ (d being diameter of either cylinder) from the inlet marked as '1' while the downstream cylinder is placed $25d$ from the pressure outlet boundary '2'. At the pressure outlet boundary, static pressure (p) is fixed equal to ambient pressure (P_∞). A uniform velocity profile is imposed at the inlet boundary with velocities along x and y -directions (u and v) taking magnitudes U_∞ and 0 respectively. The bounding walls, '3' and '4', are located $12.5d$ from cylinder center where wall effects are assumed to be negligible and the boundaries become free-slip boundaries. The cylinder walls '5' and '6' are treated differently as one is stationary while the other is rotating. No-slip boundary conditions are imposed on both the cylinders with a User Defined Function (UDF) being used for the rotating cylinder. It has been confirmed in the pre-sent study from preliminary computations that $Sc = 3.8$ at $Re = 150$. Accordingly, s is fixed equal to $5d$ for all the cases considered. The non-dimensional rotational speed, defined as $\alpha = \omega d / U_\infty$, is varied between 0 and 1. Here, ω is the angular velocity of the rotating downstream cylinder.

3. NUMERICAL SCHEME

A finite volume based commercial flow solver, ANSYS Fluent 16.0, is used for all computations in order to solve the conservation equations of mass and momentum.

- Mass conservation

$$\nabla \cdot \vec{u} = 0 \quad (1)$$

- Momentum (Navier-Stokes) conservation

$$\frac{\partial \vec{u}}{\partial t} + (\vec{u} \cdot \nabla) \vec{u} = -\frac{\nabla p}{\rho} + \nu \nabla^2 \vec{u} \quad (2)$$

Here, \vec{u} is the velocity vector, ρ is density and ν is the kinematic viscosity. Semi Implicit Pres-sure

Linked equations (SIMPLE) have been used to resolve coupling of pressure and velocity variables. The spatial derivatives are handled implicitly while a first order forward time scheme is used to discretize the temporal derivative. Second order upwind and central difference schemes have been used to discretize the convective and diffusive terms respectively. The schematic of grid for the computational domain is shown in Fig. 2 with local refinement near cylinder surfaces. Entire domain has been divided into quadrilaterals with a minimum orthogonal quality of 0.71 and maximum aspect ratio of 4.5. Grid size has been fixed after performing grid independence study by varying number of nodes on the cylinder surfaces (NC) and limiting the maximum value of aspect ratio. The results of grid independence study have been presented in Fig. 3 which clearly shows that on increasing NC beyond 100 changes in either force coefficient is less than 1%. Hence, all the computations have been carried using $NC = 100$ with a total of 110835 cells over the entire domain.

4. HILBERT-HUANG TRANSFORMATION

Hilbert spectrum, the final outcome of HHT, is the representation of complex signals on a time-frequency-energy domain that enables extraction of realistic information. The central idea behind this decomposition is the fact that in most practical scenarios frequency happens to be function of time, i.e. the fluctuations are non-stationary. This frequency is known as 'Instantaneous Frequency' (IF). Boualem (1992) and Huang *et al.* (2009) have presented detailed theory as well as importance of IF as a characteristic for interpretation of time-dependent physical phenomena. IF represents the frequency of sine wave that locally fits the given signal. However, IF makes physical sense only for mono-component signals or at the most for a narrow band of frequencies. Hence, it becomes a prerequisite to decompose any complex multicomponent signal into separate signals each of which falls in a narrow frequency range. This is achieved by the technique known as 'Empirical Mode Decomposition' (EMD). Once the component frequencies are obtained, the Hilbert Transform is

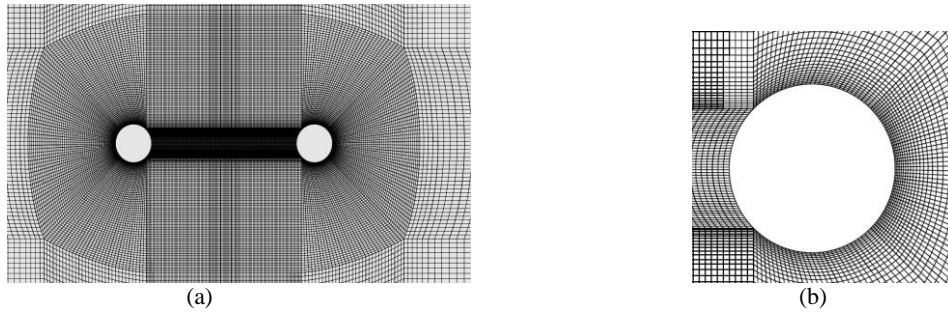


Fig. 2. (a) Schematic of grid mesh (b) magnified view of the mesh close to downstream cylinder.

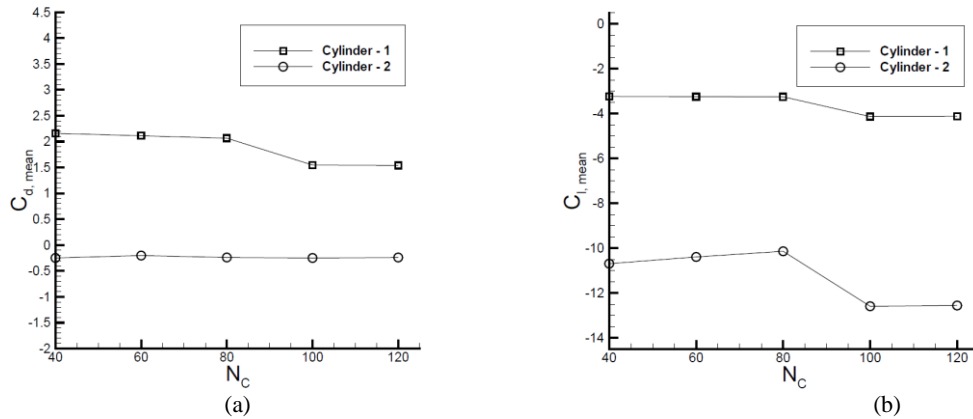


Fig. 3. Results of grid independence study (a) variation of drag coefficient (b) variation of lift coefficient, with increase in Nc.

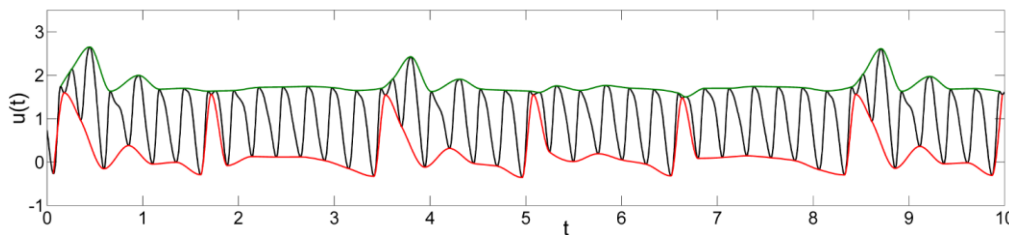


Fig. 4. Base signal along with cubic splines obtained by joining maxima and minima points.

applied separately to each component in order to extract the instantaneous frequencies. Following section briefly describes both the techniques.

4.1 Empirical mode decomposition

EMD is an intuitive technique proposed by Hunag *et al.* (1998) to extract component signals having distinct time scales from a given complex signal. Time scales are identified based on the interval between the time instants corresponding to occurrence of local maxima and minima of the signal. Each of these decomposed signals is known as 'Intrinsic Mode Function' (IMF) and obeys a set of conditions that enable their extraction from the base signal. The algorithm to extract the IMFs from an arbitrary signal, $u(t)$, is as follows. Here $u(t)$ could be considered as fluctuation in computed values of streamwise velocity in wake of the downstream cylinder that spans over a time interval of 10 seconds.

The first step in EMD is construction of two cubic splines, one joining maxima points and other minima points of $u(t)$. These curves, denoted as $u_{max}(t)$ and $u_{min}(t)$, are shown in Fig. 4 as the enveloping and limiting cubic splines. Once the limiting curves are obtained, the mean function can be defined as

$$m(t) = \frac{u_{max}(t) + u_{min}(t)}{2} \quad (3)$$

Now the first signal that could be an IMF, denoted by $h(t)$, is defined as

$$h(t) = u(t) - m(t) \quad (4)$$

This operation is named 'shifting' because at the end of operation the new signal $h(t)$ contains fluctuations of $u(t)$ that shift towards zero mean as shown in Fig.5. The obtained signal $h(t)$ would become an IMF only if the signal is completely shifted to zero mean. This is achieved by sequential

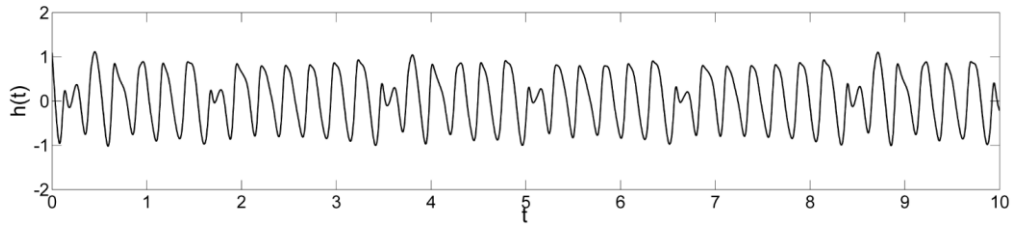


Fig. 5. Signal obtained after the first shifting operation.

iterations where $u(t)$ is replaced by $h(t)$ in all the previous steps till $m(t) \approx 0$. Finally, $h(t)$ that meets this requirement is the first IMF and is denoted as $C_1(t)$. Thus, $C_1(t)$ can be expressed as

$$C_1(t) = h(t), \text{ when, } m(t) \approx 0 \quad (5)$$

Once an IMF is obtained, it is subtracted from the original signal $u(t)$ to obtain the residue signal $r(t)$ as follows.

$$r(t) = u(t) - C_1(t) \quad (6)$$

This residue is used for extraction of remaining IMFs. The process is repeated until $r(t)$ becomes monotonic after consecutive extraction of IMFs from the base signal. The sample signal ($u(t)$)

obtained from present computations has been decomposed into 7 IMFs as shown in Fig. 6. The accuracy of decomposition can be ascertained by summing up all the IMFs and comparing it with the original signal. Ideally, Eqn. (7) must be satisfied to which small deviations may appear due to non-orthogonality of signals, spline fitting and information loss in residues. By putting control checks on this deviation, the correctness of EMD can be assured.

$$u(t) = \sum_{i=1}^6 C_i(t) \quad (7)$$

Figure 7 shows variation of the two signals, viz. summation and residue, and makes it evident that EMD effectively decomposes $u(t)$ into component signals of frequency scales. However, the figure clearly illustrates that there is deviation in the mean value of the signal due to the mono-tonic residue that is left behind after EMD. Variation of residue is also shown in the figure to confirm that addition of residue on RHS of Eqn. (7) would yield exact overlap of both the signals except slight deviations at the edges. This is due to the end effects caused by extrapolation of data after each shifting operation. This has to be done in order to preserve the sample length.

4.2 Hilbert Spectra

The Hilbert transform provides a complex analytic representation of an arbitrary signal preserving its form and energy. This feature is vital for extraction of instantaneous frequency. The Hilbert transform, $H(t)$, of a signal $u(t)$ is defined as

$$H(t) = \frac{1}{\pi} PV \int_{-\infty}^{\infty} \frac{u(t')}{t-t'} dt' \quad (8)$$

Where, PV refers to 'principal value'.

Thus the analytic function can be expressed as $Z(t) = u(t) + iH(t) = a(t)e^{i\theta(t)}$. The base signal forms the real part while the transform constitutes the complex part. The instantaneous frequency, $f(t)$, can be obtained from the relation

$$f(t) = \frac{d\theta(t)}{dt} \quad (9)$$

where, $\theta(t)$ is the phase difference between the real and imaginary part of the analytic function and is given by

$$\theta(t) = \arctan\left(\frac{u(t)}{H(t)}\right) \quad (10)$$

It should be noted that $\theta(t)$ needs to be unwrapped before performing differentiation mentioned in Eqn. (10) in order to eliminate discontinuity caused by phase jump. Energy associated with the signal can be obtained from the amplitude, $A(t)$, of $Z(t)$ and is expressed as

$$A(t) = \sqrt{u(t)^2 + H(t)^2} \quad (11)$$

Equations (8) and (9) combine to establish the Hilbert energy spectrum, $H(f,t)$, that conveys information about their behavior in energy-frequency-time plane. It is possible to describe the instantaneous energy spectrum and mean marginal spectrum from the Hilbert transform by integrating $H(f,t)$ about the frequency and time domains respectively. Instantaneous energy spectrum provides information about the energy fluctuations and is expressed as

$$IE(t) = \int_f H(f,t) df \quad (12)$$

The mean marginal spectrum $M(f)$ is analogous to Fourier spectra and provides information about the energy contribution of component frequencies. It is expressed as

$$M(f) = \frac{1}{T} \int_0^T H(f,t) dt \quad (13)$$

Here, T denotes the total sampling time. The main advantage of HHT over conventional Fourier

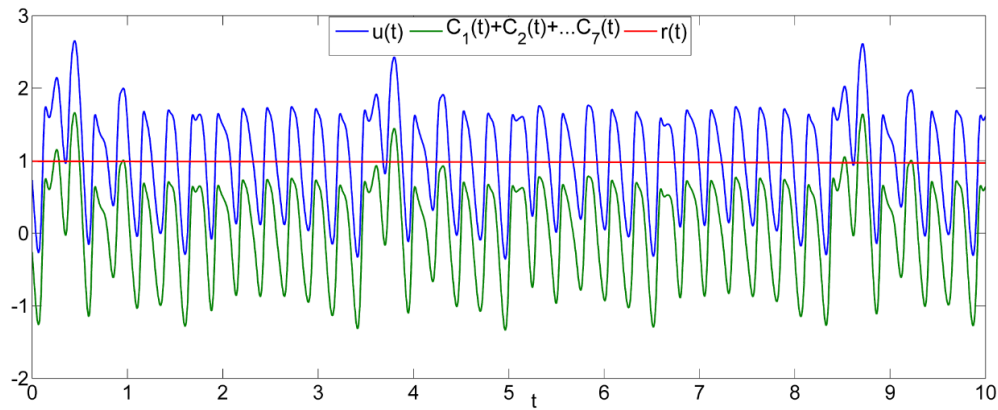


Fig. 6. $C_1(t)$ to $C_7(t)$ represent the IMFs after empirical mode decomposition of $u(t)$.

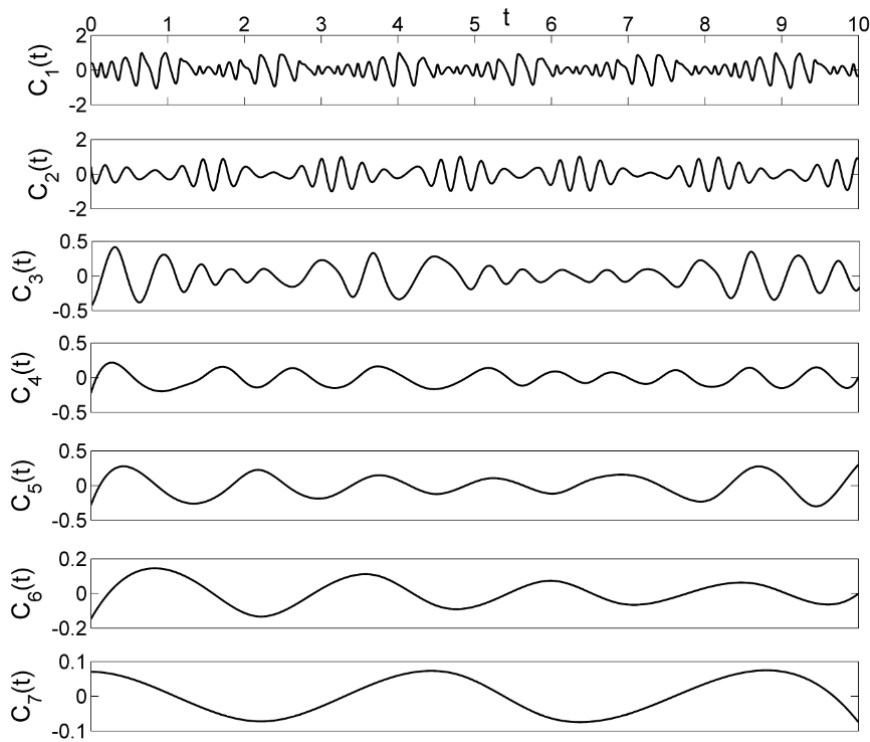


Fig. 7. Comparison of $u(t)$ with summation of 7 IMFs.

transform lies in its ability to accurately describe non-stationary fluctuations. Hence, it is necessary to quantify the 'Degree of Stationarity', $DS(f)$, of a signal which can be expressed as

$$DS(f) = \frac{1}{T} \int_0^T \left(1 - \frac{H(f,t)}{M(f)} \right)^2 dt \quad (14)$$

5. RESULTS AND DISCUSSION

5.1 Validation of Computations

Numerical scheme used for simulations has been validated by comparing its results with two benchmark fluid flow problems, namely, flow past rotating circular cylinder and flow past two stationary tandem circular cylinders.

The lift coefficient (C_l), drag coefficient (C_d) and Strouhal number (St) obtained for the case of flow past rotating circular cylinder have been compared with results reported in literature for fixed non-dimensional rotational speed, $\alpha = 1$, and two different values of Re , viz. 100 and 200. The results presented in Table-1 show close match with those cited from literature.

Figure 8 presents the variation of mean drag coefficient for upstream and downstream cylinders with variation in inter-cylinder spacing for flow past stationary inline circular cylinders. The results are compared with those of [Meneghini and Saltara \(2001\)](#) and [Slauti and Stansby \(1992\)](#). Error bars have been presented in this figure from mean of drag values coefficient values reported in literature

and present computation. The width of these error bars have been chosen as the maximum deviation between results reported in literature. It is evident that the trends as well as the magnitudes of drag variation have been adequately captured by the present computations within permissible error limits. The subscripts 1 and 2 in Fig. 8 refer to upstream and down-stream cylinders respectively.

Table 1 Validation of force coefficients and Strouhal number for flow past a rotating circular cylinder

	Re	α	C_l	C_d	St
Kang et al. (1999)	100	1	-2.4833	1.097	0.165
Present	100	1	-2.485	1.101	0.165
Kumar et al. (2011)	200	1	-	-	0.195
Mittal and Kumar (2003)	200	1	-2.375	1.09	0.190
Present	200	1	-2.375	1.104	0.192

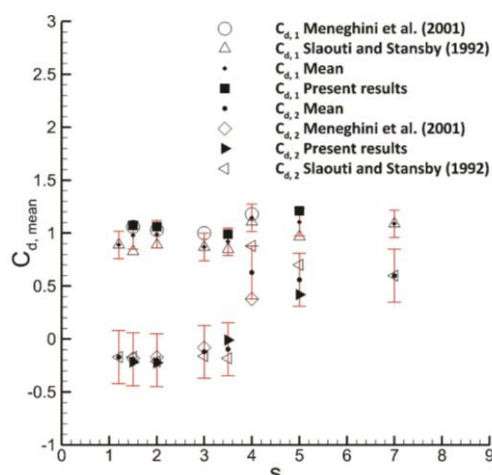


Fig. 8. Variation of mean drag coefficient with increase in inter-cylinder spacing for flow past two stationary tandem circular cylinders.

5.2 Wake characteristics

The instantaneous z -vorticity contour over the parametric range of rotational speed is presented in Fig. 9. The transformations in vortical structures depicted in these results as α varies from 0-1 confirm transitions in temporal characteristics of the wake. The classic braided periodic vortices observed at $\alpha = 0$ lose symmetry about the line $y = 0$ due to upward tilt induced by clockwise rotation of the downstream cylinder. Such a motion is anticipated to shift the vortex street in the positive y -direction as reported by Mittal and Kumar (2003). However, it is observed that the tilt of wake is not significant up to $\alpha = 0.5$. For $\alpha \leq 0.5$, vortices from the downstream cylinder are shed in the

positive y -direction while vortices from the

upstream cylinder are shed in the negative y -direction resulting in a wider wake rather than a tilted one. The interaction between these vortices also changes with change in rotational speed. At $\alpha = 0$, vortex shedding from the down-stream cylinder is triggered by the shedding from upstream cylinder and their frequencies are found to be synchronous. However, with increase in α , the interaction become more complex. This is affirmed by the presence of multiple peaks in time series signals of lift and drag coefficients for downstream cylinder as shown in Fig. 10.

An increase in α is accompanied by downstream shift in pinch-off location of vortices from the upstream cylinder. This is because the rotation of downstream cylinder causes shear layers from upstream cylinder to stretch further downstream delaying the detachment of vortices. In fact, beyond $\alpha = 0.62$, such stretching of the shear layer eventually results in arrest of vortex shedding from the upstream cylinder as shown in Fig. 9. For values α equal to 0.75 and 0.87, only anti-clockwise vortices are shed while the clockwise shear layer begins to wrap around the anti-clockwise shear layer. With further increase in α , these shear layers completely wrap around one another forming a spiral resulting in arrest of vortex shedding as observed for $\alpha = 1$. Similar observations regarding suppression of vortex shedding have been reported by Mittal and Kumar (2003) in case of flow past a rotating circular cylinder.

Figure 10 depicts the temporal evolution of lift and drag coefficients for the downstream cylinder over a flow time of 10 seconds. The cascading of lift coefficient signals occurs due to progressive pressure imbalance on either surface of the cylinder as a result of its rotation.

Another observable characteristic is increase in amplitude and time period of the signals with increase in α . Multiple peaks in these signals at larger values of α suggest non-linearity and non-stationarity of signals. Since these forces are predominantly influenced by the wake characteristics, it could be inferred that the interplay between pulsation induced by vortex shedding from the upstream cylinder and circulation effect of downstream cylinder due to its rotation tends to become complex. Detailed investigations on these aspects with the help of HHT are presented in the following subsections.

5.3 Degree of Stationarity

HHT is capable of disclosing the degree of nonlinearity in transient signals that appears in the form of inter-wave and intra-wave modulations (features of non-stationarity). However, it would be best to estimate the scale of nonlinearity in the time series signals before examining their spectra. Hunag *et al.* (1996) have proposed a statistical measure to quantify the Degree of Stationarity, i.e. $DS(f)$ of a fluctuating signal as described by Eqn. (14). This

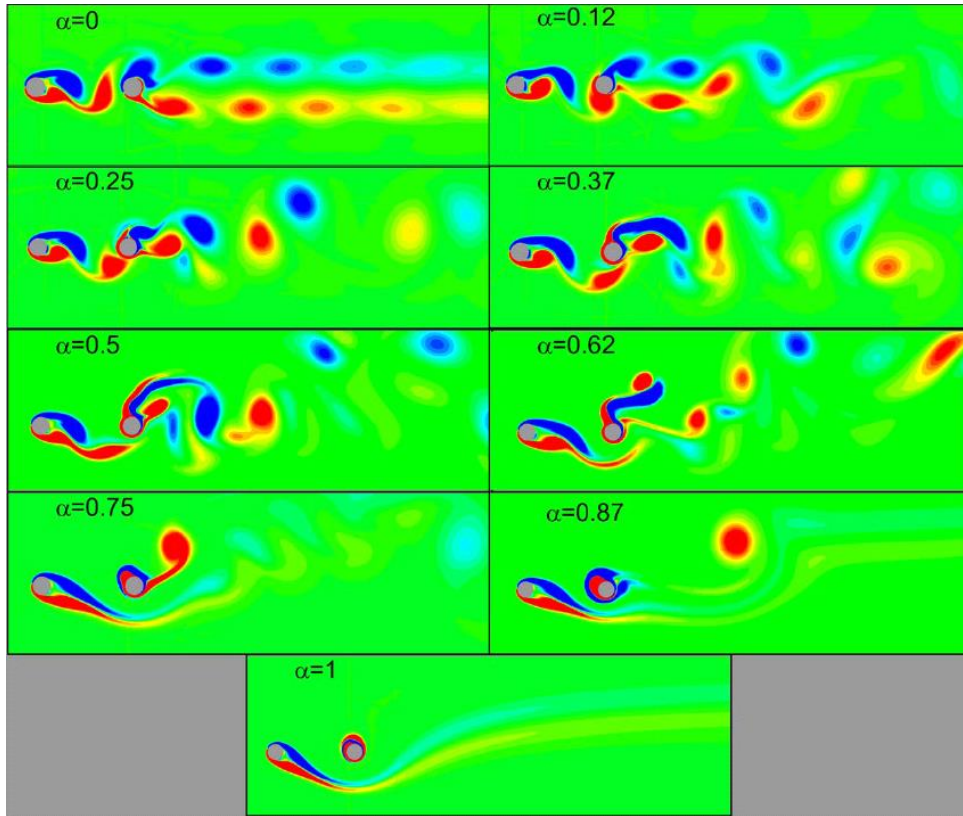


Fig. 9. Instantaneous vorticity contours for different values of α .

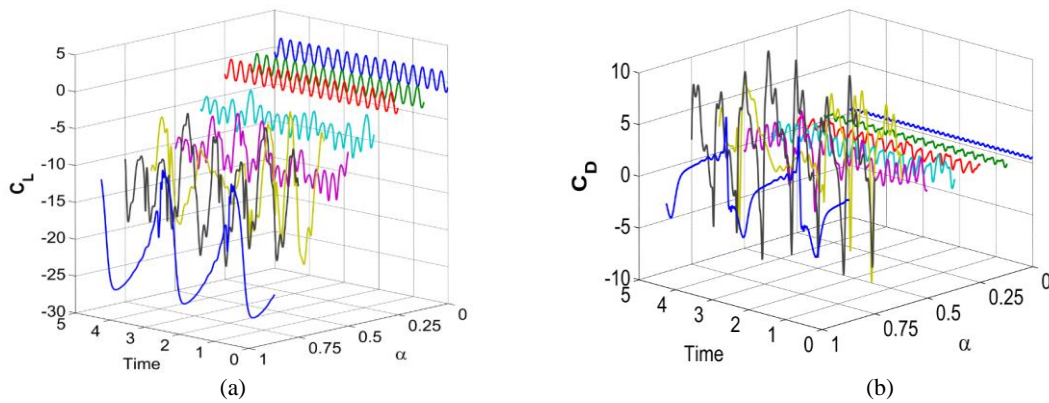


Fig. 10. Temporal variation of drag and lift coefficients for the downstream cylinder.

expression essentially represents the deviation of mean marginal spectrum, $M(f)$, from the corresponding Fourier spectrum, $F(f)$. For example, if the signal contains only a single frequency sine or cosine wave of constant amplitude throughout the sampling time then the corresponding $F(f)$ and $M(f)$ would be identical and $DS(f)$ would be zero. The Fourier spectra depict energy distribution of sine or cosine waves present in a signal that exist over the entire sampling time. On the other hand, the energy-frequency distribution of HHT is a local concept and finds the probability of such a wave to exist

within a small time-frequency window.

The $DS(f)$ of the lift signal over range of α values are presented in Fig. 11 (a). The results clearly illustrate a progressive increase in non-stationarity of the signals with increase in α . In absence of rotation, $DS(f)$ is almost zero indicating a close match to sine or cosine waveform. However, with increase in rotational speed, the local behavior becomes prominent and use of Fourier analysis to describe such fluctuations becomes less physical. The intermittent spikes clearly point to modulations present in the signal that may be caused by phase, frequency or amplitude shift. Figure 11(b) reveals

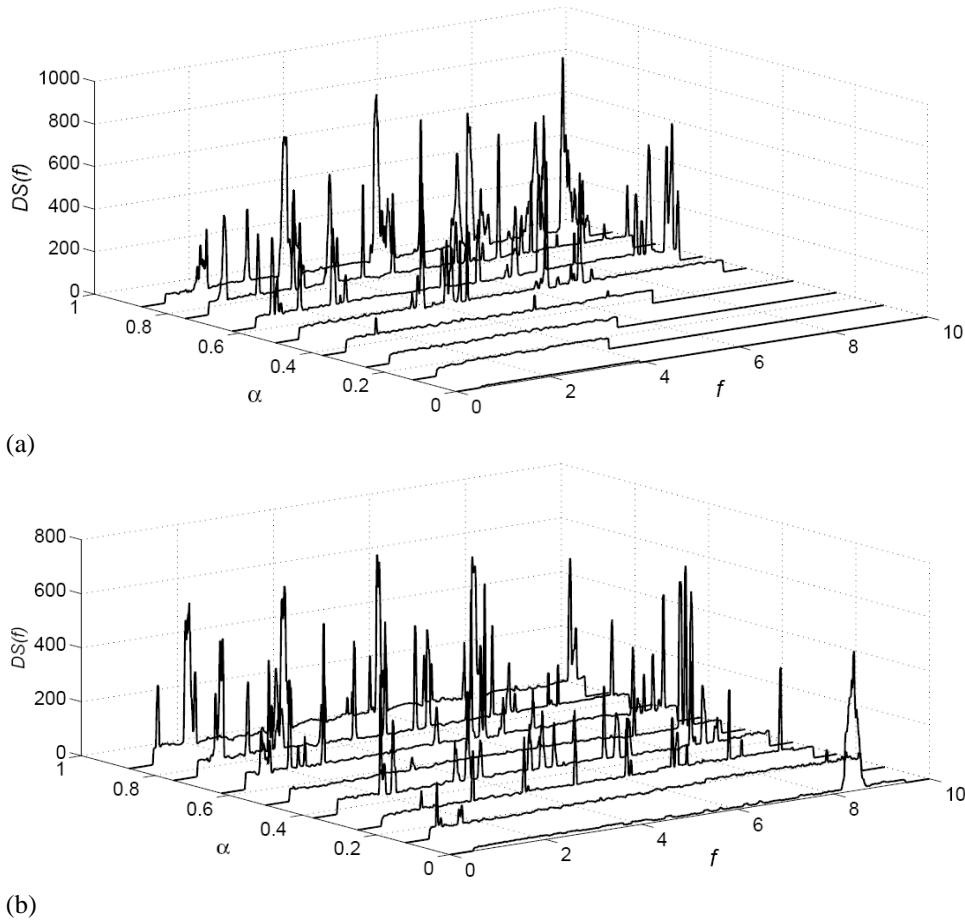


Fig. 11. Degree of stationarity ($DS(f)$) for different values of α in (a) lift (b) drag signals.

the nature of variation of $DS(f)$ for the drag signal with change in α and f . It is apparent from the figure that contrary to behavior of lift signal, there exists non-stationarity in drag signal even in absence of rotation at frequencies close to 8. This is due to vortex-to-vortex and vortex-to-cylinder interactions in the inter-cylinder gap that cause relatively larger distortion in streamwise velocity signals. Further clarity regarding frequency distribution would be revealed by the Hilbert spectrum. The spikes in $DS(f)$ also appear to be uniformly spaced in the frequency plane for small values of α suggesting harmonic and sub-harmonic superposition.

5.4 Hilbert Spectra

The Hilbert energy distribution of the lift signal of downstream cylinder for different rotational speeds has been presented in Fig. 12. A Gaussian filter with 0.5 weightage has been applied over 10×10 window to smoothen the spectra for continuity. This figure depicts the energy contribution of IMFs obtained from EMD. In case of stationary cylinders, there is just one IMF with a mean instantaneous

frequency of 3.8 Hz, indicating closeness to single harmonic nature. This frequency is synchronous with the shedding frequency of upstream cylinder

indicating that upstream oscillations trigger vortex shedding from the downstream cylinder. However, with an increase in rotational speed up to $\alpha = 0.5$, distinct low-frequency IMFs emerge as observed from Fig. 12. The occurrence of such large wavelength signals points to alteration of flow structure in the inter-cylinder space. The energy density indicated by color levels in the contour shows that the most prominent signal still has mean frequency close to 3.8 Hz, suggesting an influence of vortex shedding from upstream cylinder on downstream wake. The amplitude of the dominant IMF, which represents the frequency spread of signal, is also found to increase with increase in rotational speed. This essentially confirms a simultaneous increase of intra-wave modulation with rotational speed. For α values of 0.62 and 0.75, the spectra are hazy with occasional spikes of high frequency. The IMFs are no longer distinct because of strong inter-wave and intra-wave modulations which gives evidence of a complex wake. For $\alpha = 0.87$, the Hilbert spectra appear to be more ordered with high frequency spikes at regular intervals. This time period is found to match with the highest energy frequency of the base signal presented in Fig. 10. Such physical attributes are easily revealed by use of Hilbert spectra with ease because of locally defined instantaneous frequencies. The sudden increase in amplitude of

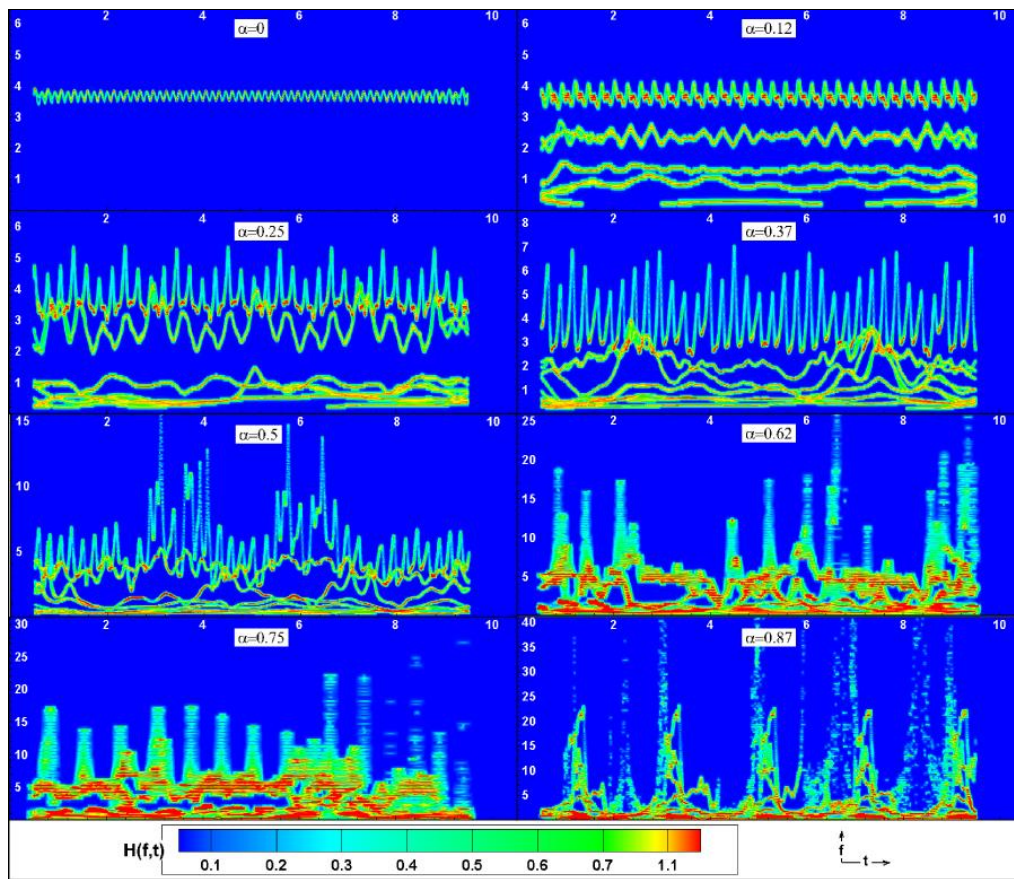


Fig. 12. Hilbert spectra of downstream cylinder lift for different values of α .

the lift signal presented in Fig. 10 transmutes in the form of high instantaneous frequency spike in the Hilbert spectra.

The Hilbert spectra of drag forces on the downstream cylinder are presented in Fig. 13. As explained in the previous section, the streamwise component of force is greatly affected by the transformations of fluid structures in the inter-cylinder space thereby creating modulations in the force coefficient signals. The spectra of the stationary case show a distinct IMF in the instantaneous frequency range 6.2-8.15 Hz. Apart from this component, certain low-frequency components are also observed along with a high-frequency spike at $t=0.82$. Spectra of the drag signals also reveal that an increase of rotational speed results in more complex and less ordered flow akin to observations from lift signal. The peaks of instantaneous frequency are found to increase from 12 Hz for $\alpha=0$ to 23 Hz for $\alpha=0.87$ while there occurs shift of energy density towards lower frequencies. The modulations and intertwining of IMFs at α values of 0.62 and 0.75 are clear indicators of underlying nonlinear mechanisms. However, Figs.12 and 13 show visible recovery of dynamic stability at $\alpha=0.87$ and the flow becomes steady at $\alpha=1$. The spectra show uniformly spaced spikes of high instantaneous frequency and energy density at $\alpha=0.87$. This is indicative of a shift in the temporal behavior of the

flow. Since the time gap between the uniformly distributed spikes is large, it can be inferred that the IMFs in low frequency range having large wavelengths become dominant at larger values of α . The development of strong shear layer that tends to wrap the rotating cylinder could be the cause of this re-stabilization.

5.5 Marginal Spectral Distribution

Frequency energy density distribution of drag and lift signals are presented in Figs. 14 (a) and (b) respectively for different value of rotational speed. Even though HHT is known to be effective in identifying significant low-frequency components in a signal, it is prone to generation of stray low-frequency components that arise from extrapolation operations performed to overcome end effects. These aspects have been detailed in Huang (2014). In present computations, to minimize this effect, a cutoff frequency has been set as 0.3 Hz which is one-third of the minimum frequency that could be identified from the chosen sample width. At $\alpha=0$, two frequency ranges can be identified in the marginal spectra of drag signals in Fig. 14 (a), one close to 0.35 Hz and another spread over 6.2-8.15 Hz. However, Fourier spectra for the same signal show only a single peak at 7.3 Hz as shown in Fig. 14 (a). This deviation in results indicates an upper edge of HHT because it is able to identify modulation in the frequency range of 6.2-8.15 Hz. The waveform of the actual signal has been

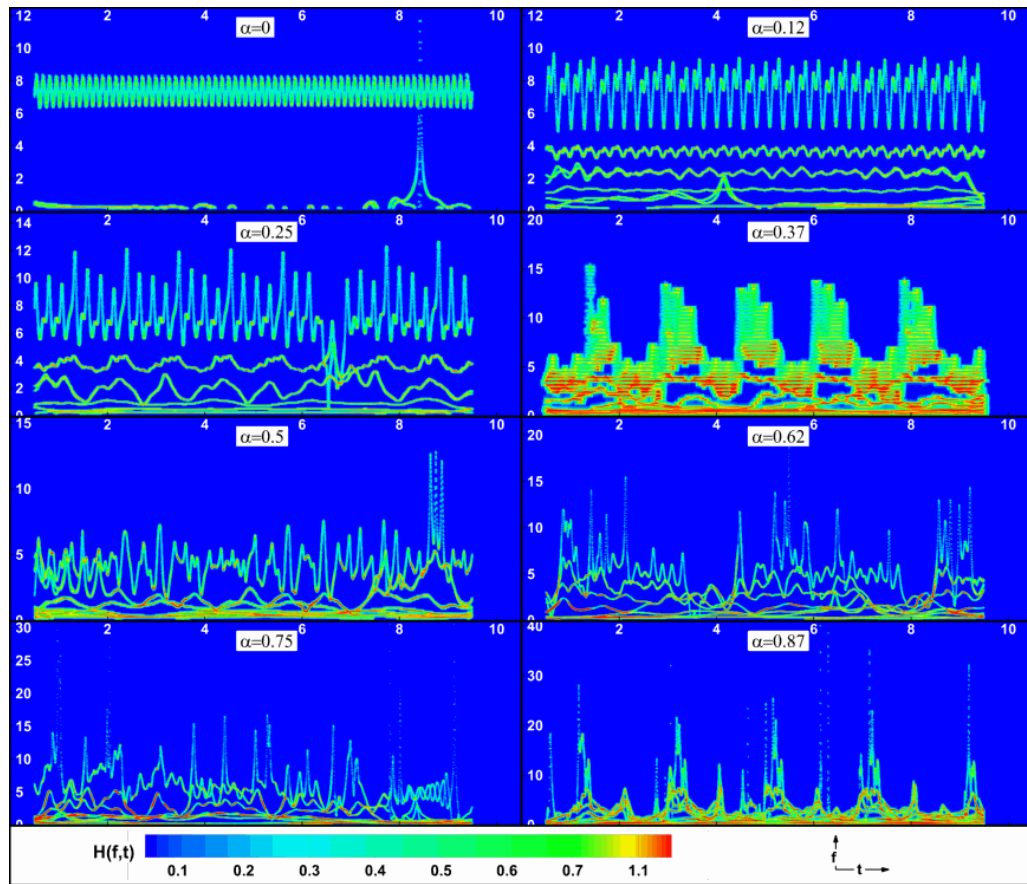


Fig. 13. Hilbert spectra of downstream cylinder drag for different values of α .

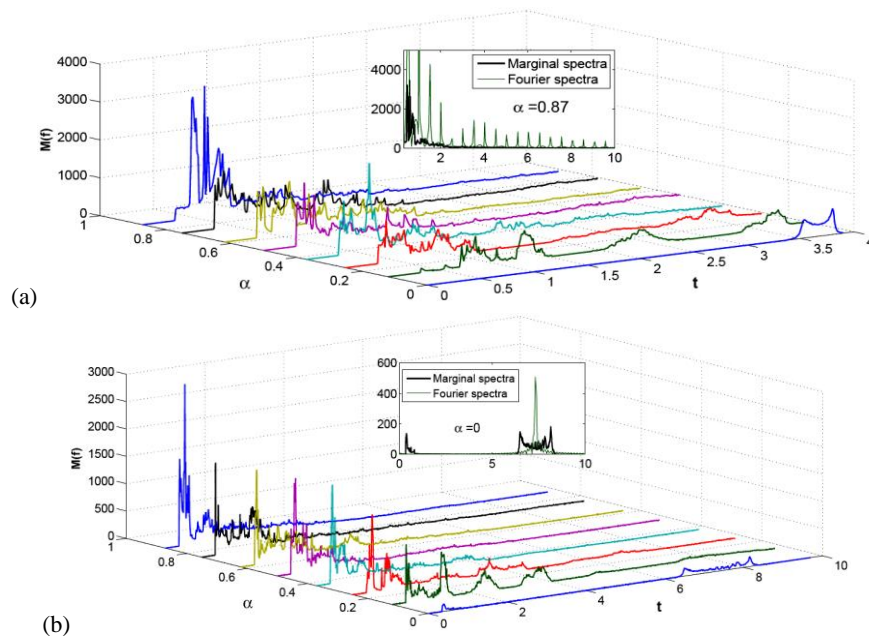


Fig. 14. Marginal spectral distribution of (a) drag signals (b) lift signals, for different value of rotational speed α .

compared with a sine wave of single frequency and is found to be dissimilar revealing intra-wave modulations. A similar comparison between the two spectra at $\alpha = 0.87$ is presented in Fig. 14 (b). Here

the Fourier spectra reveal existence of multiple harmonics while the marginal spectra show contributions from signals with frequencies in the range 0-2 Hz. Thus, even though both the spectra

show maxima at frequencies close to 0.5 Hz, it is evident that marginal spectra bring out contribution from wider band of frequencies.

Spectra of C_l as well as C_d reveal a shift in energy density towards lower frequencies with increase in rotational speed. Frequency bands corresponding to each IMF are identified in the form of hunches in the marginal spectra. However, these become less distinct and merge to form a continuous band at higher values of rotational speed.

6. CONCLUSION

Effect of rotating downstream cylinder on temporal characteristics of flow past two inline circular cylinders has been investigated for $Re = 150$ and $s = 5d$. The non-dimensional rotational speed of the downstream cylinder has been varied between 0 and 1 for which the flow exhibits periodic, non-periodic and steady behavior. The nature of unsteadiness has been analyzed using Hilbert-Huang transformation and results are presented in the form of contours and energy spectra. It is found that this technique having ability to effectively decompose non-stationary signals delivers better insight into flow physics as compared to conventional Fourier analysis. Even in absence of rotation of downstream cylinder, a measure of degree of stationarity of the drag signal reveals non-linear interactions in flow which do not get effectively captured by Fourier analysis. It is also found that increase of rotational speed is accompanied by an increase in the inter-wave and intra-wave modulations of the time series signals, suggesting growth of nonlinear interactions in the wake. However, the flow becomes steady beyond a critical rotational speed for which transition corresponds to wrapping of the downstream cylinder by its shear layers. Although the present study investigates data from numerical simulation, HHT could be used for analysis of experimental data as well. Literature indicate its application in de-noising experimental data. In brief, results from present study suggest that HHT is an efficient tool for analysis of transient flows, especially in the transitional regime where the flow interactions become nonlinear.

REFERENCES

- Bearman, P. W. (2011). Circular cylinder wakes and vortex-induced vibrations. *Journal of Fluids and Structures*. 27(5), 648-658.
- Boashash, B. (1992). Estimating and interpreting the instantaneous frequency of a signal. I. Fundamentals. *Proceedings of the IEEE*. 80(4), 520-538.
- Carmo, B. S. and J. R. Meneghini (2006). Numerical investigation of the flow around two circular cylinders in tandem. *Journal of Fluids and Structures*. 22(6), 979-988.
- Huang, N. E., Z. Shen and S. R. Long. (1999). A new view of nonlinear water waves: the Hilbert Spectrum 1. *Annual review of fluid mechanics*. 31(1), 417-457.
- Huang, N. E. (2014). *Hilbert-Huang transform and its applications* 16. World Scientific.
- Huang, N. E., Z. Shen, S. R. Long, M. C. Wu, H. H. Shih, Q. Zheng, N.C. Yen, C. C. Tung and H. H. Liu (1998). The empirical mode decomposition and the Hilbert spectrum for nonlinear and non-stationary time series analysis. *Proceedings of the Royal Society of London A: Mathematical, Physical and Engineering Sciences*. 454, 903-995.
- Huang, N. E., Z. Wu, S. R. Long, K. C. Arnold, X. Chen and K. Blank (2009). On instantaneous frequency. *Advances in adaptive data analysis*. 1(2), 177-229.
- Igarashi, T. (1981). Characteristics of the flow around two circular cylinders arranged in tandem: 1st report. *Bulletin of JSME*. 24, 323-331.
- Immanuvel, P., K. Arul Prakash and S. Vengadesan (2014). Onset of laminar separation and vortex shedding in flow past unconfined elliptic cylinders. *Physics of Fluids*. 26(2), 023-601.
- Kang, S., C. Haecheon and L. Sangsan (1999). Laminar flow past a rotating circular cylinder. *Physics of Fluids*, 11:11, pp. 3312-3321.
- Kumar, S., C. Cantu and B. Gonzalez (2011). Flow past a rotating cylinder at low and high rotation rates. *Journal of Fluids Engineering*. 133(4), 041201.
- Meneghini, J. R., F. Saltara, C. L. R. Siqueira and J. A. Ferrari (2001). Numerical simulation of flow interference between two circular cylinders in tandem and side-by-side arrangements. *Journal of fluids and structures*. 15(2), 327-350.
- Mittal, S. (2001). Control of flow past bluff bodies using rotating control cylinders. *Journal of fluids and structures*. 15(2), 291-326.
- Mittal, S. and K. Bhaskar (2003). Flow past a rotating cylinder. *Journal of Fluid Mechanics*, 476(4), 303-334.
- Mizushima, J. and N. Suehiro (2005). Instability and transition of flow past two tandem circular cylinders. *Physics of Fluids*. 17(10), 104-107.
- Shaafi, K. and S. Vengadesan (2014). Wall proximity effects on the effectiveness of upstream control rod. *Journal of Fluids and Structures*. 49, 112-134.
- Slaouti, A. and P. K. Stansby (1992). Flow around two circular cylinders by the random-vortex method. *Journal of Fluids and Structures*. 6(6), 641-670.
- Sun, Z., J. Zhou and P. Zhou. (2006). Application of Hilbert-Huang transform to denoising in vortex flowmeter. *Journal of central south university of technology*. 13 (5), 501-505.

